Chapter 6

Fully polarimetric bistatic scattering measurements from vegetation and simulation using modified first-order radiative transfer model at C band

6.1 Introduction

Interpretation and modeling of polarimetric bistatic radar response of targets such as vegetation, land surfaces, forest, snow, and the ocean is gaining importance in the field of active microwave remote sensing. The problem, including target scattering decomposition and retrieval of desired physical parameters of the targets utilizing bistatic radar returns, has attained significant importance as more bistatic radar missions are investigated. The initial technical results of the first functional bistatic/multistatic radar operation were demonstrated by the TanDEM-X mission [34]. However, TanDEM-X has geometries with short baselines that can be considered quasi-monostatic. The direct and quasi-

specular reflected data of Global Navigation Satellite System- Reflectometry (GNSS-R) acquired using ground/airborne GNSS-R systems under slightly different from the backscattering concept has been studied for larger biophysical and land geophysical applications parameters retrieval [157–159]. In contrast, the recent bistatic and companion satellite missions such as the SESAME, the SAOCOM, and Harmony (Phase-A study of the Earth Explorer 10 mission candidate) have a larger baseline and significant bistatic angle consideration (i.e., greater than 20°) [32, 35, 36].

The polarimetric signatures of radar bistatic scattering mechanism depend on the target's physical properties, the target's orientation with respect to the transmitter and receiver baseline, polarization orientation, frequency, zenith, and azimuth angle. The cost challenges, synchronization of transmitter and receiver at a different location, the sizeable outdoor field requirement for small-scale testing of the ground and airborne bistatic radar system, and mathematical challenges for developing a microwave scattering model for a different target are the complexities in the implementation of space-borne bistatic missions. However, the higher degree of freedom of the bistatic configuration provides flexibility to system design and better interpretation of the target's polarimetric signatures with physical meaning. The stronger radar return of the target can be achieved by optimizing the bistatic radar system that can help advance the future bistatic/multistatic space-borne missions.

Most of the polarimetric bistatic observable quantities for land bio-geo physical applications are initially demonstrated using TanDEM-X and GNSS-R techniques [33, 34]. However, very few ground-based optimizations of bistatic specular configurations confirmed the sensitivity of time-series polarimetric radar returns signature from vegetation to vegetation biophysical parameters [44, 45, 160]. Furthermore, to our knowledge, none of the scientific works have been done on the sensitivity time-series fully-polarimetric bistatic scattering to a vegetated rough soil surface. Despite the first successful demonstration of emerging techniques for mapping global soil moisture field using GNSS-R by [161],

vegetation's biophysical retrieval by [162, 163], land geophysical parameter retrieval by [133, 164], tropical wetlands mapping by [165] and potential of flood mapping by [166], the methodological challenges are yet challenging and interesting to solve for bistatic configurations.

A significant number of methodologies for bistatic microwave scattering were developed to visualize the interaction of microwave signals with different targets like a forest, agricultural crops, bare lands, snow, oceans, etc., and their physical parameter retrieval [45, 54, 119, 144, 167–172]. Most of the theoretical models for inhomogeneous mediums such as small-height vegetations, agricultural fields, forests, and bare lands are broadly divided into incoherent and coherent scattering models. Further, the incoherent approaches for multiple scattering components by an inhomogeneous medium are classified into two (1) Analytical theories; and (2) Transport theories. The analytical approach uses the wave and maxwells equation to investigate multiple scattering components, interference, and diffraction effects between electric fields and inhomogeneous medium. This approach is mathematically complex and time-consuming. In contrast, the transport theory deal with energy transfer through a medium containing scattering particle. This theory assumes no correlation between fields scattered by the scattering constituents that allows the consideration of the incoherent addition of the power associated with multiple scattering components. However, the coherent scattering model deals with the coherent sum of complex scattered fields from scattering constituents with the same propagation phase delays and specular reflection phase changes.

In this study, we have proposed the synergy of the rough soil surface scattering model within the vector radiative transfer theory-based vegetation scattering model in the bistatic specular direction. The Kirchhoff approximation is used to model scattering from a bare rough surface. The proposed model allows incoherent addition of single and multiple scattering contributions through vegetation overlaying rough soil surface. The model

does not include the coherence effect since the coherent effect within total scattering is considered insignificant for higher frequencies such as X and C bands. The proposed microwave scattering model simulates temporal variation of bistatic scattering from wheat crop overlaying rough soil surface. In addition, the decomposition of single and multiple scattering components allows the interpretation of dominant scattering contributions with age. Furthermore, the validation of the theoretical scattering model with the experimental results enables the development of scattering models, which are useful for making predictions with quantified confidence and high predictive accuracy.

6.2 Experimental data collection methods

The bistatic scatterometer (BiSCAT) measurements in the forward specular plane for vegetation overlying soil surface are carried out at the Department of Physics, IIT (BHU), Varanasi, India $(82°59'34''E, 25°15'32''N)$. The fully polarimetric (i.e., HH, VV, HV, and VH) C band time-series bistatic scattering responses are measured using the BiSCAT system. The experimental arrangement of the designed bistatic scatterometer system is shown in Figure 5.1 of Chapter 5. The wheat crop bed of area $10m \times 10m$ is specially prepared for the BiSCAT observations. The BiSCAT observations are taken for different phenological stages of wheat crop starting from 20^{th} January 2020 (20 Days after sowing) till 27^{th} March 2020 (87 Days after sowing) at the interval of 8-10 days. The in-situ observations such as plant water content (PWC), plant height (d), volumetric soil moisture (m_v), surface root mean square height (s), and correlation length (l) are taken on each date of the BiSCAT measurement for the accurate characterization of the measured Bistatic scattering coefficients (σ^0_{pq}) dependencies on the soil surface and vegetation biophysical parameters. The PWC, m_v, and d are measured such that the soil and crop conditions within the Radar field of view (RFOV) of the C band antenna are undisturbed.

6.2.1 Technical information of the C band Bistatic scatterometer system

The E82578D, PSG high power Radio Frequency instrument is used in the BiSCAT system to generate continuous microwave signals ranging from 10MHz to 20GHz. The Agilent technologies make Power sensors (E9327A, -60 to 20 dBm, 50 MHz to 18 GHz) connected to power meter of series EPM-P (E4416A, -70 to 44 dBm, 9 kHz to 110 GHz) are used to observe bistatic scattering power through different phenologies of wheat crop overlaying rough soil surface. Two pairs (i.e., transmitting and receiving) of WR-159 standard gain horn antenna for C band (operating range from 4.9 GHz to 7.05 GHz) are arranged in a specular plane and mounted on a 10-meter horizontal railing track at the height of 3-meter from the soil surface. The power sensor sensed the power scattered in a specular direction. The average scattered power per unit area from the target in a specular direction is further used to compute the value of fully-polarized σ^0_{pq} using the radar equation [3]. The horizontal and vertical beamwidth for the C band horn antenna is 14.3° and 16.9°, respectively. The antennas are attached to the rotator for a change in viewing zenith angle with a rotating precision of 1°. This study does not have azimuth variation in the σ^0_{pq}. The transmitting and receiving antenna positions for the forward specular zenith angle variation from 20° to 60° at the interval of 10°) from the center of the horizontal railing track were synced using the lasers.

The fully-polarized bistatic scattering coefficient is measured at a central frequency of 6 GHz. The measurements are made at a wide specular incidence angular range varying from 20° to 60° at the interval of 10°. The experiment is repeated four times, each day of the BiSCAT measurements to compute the average values of σ^0_{pq} at HH, VV, HV, and VH polarizations. After every measurement, the BiSCAT system was calibrated by adapting the polarimetric calibration technique. The calibration was conducted carefully on a specifically designed concrete horizontal surface beside the sampling field using similar

technical specifications as the BiSCAT system. An aluminum sheet larger in size than C band RFOV is placed parallel on a horizontal surface, which is used as a calibration target. The necessity of calibration is to obtain meaningful information from time-series σ^0_{pq} such that the target scattering response is dependent on the frequencies, polarizations, and specular incidence angle, and the structural and physical properties of vegetation and land surface parameters. The variation in the measured value of σ^0_{pq} from its mean is found between 0.07 to 0.42.

6.2.2 Vegetation and land surface parameter measurements

Fig. 6.1 Condition of different phenological stages of wheat crop during the BiSCAT measurements.

The insitu observations, such as vegetation biophysical (i.e., PWC and d) and soil surface parameters (m_v, s, and l), were taken concurrently with each day of the BiSCAT measurement. The phenological stages of the wheat crop at which the in-situ observations and the BiSCAT measurements occurred are shown in Figure 6.1. A meter scale was set at five different locations within the sampling field to measure the plant heights of the wheat crop. The destructive sampling method is used to measure the weight of the fresh vegetation biomass ($W_{Fresh\ veg}$). For every in-situ observation, the five vegetation samples are collected from the sampling field outside the horn antennas RFOV. The fresh

vegetation sample is further dried in an oven at 60° for 72 hours to compute the dry weights of vegetation samples ($W_{dry\ veg}$). Furthermore, the fresh and dry weights of vegetation samples are used to compute average values of PWC utilizing Equations 6.1.

$$PWC = [\frac{1}{5}\sum_{i=0}^{5}(W_{Fresh\ veg} - W_{Dry\ cluster_i})]\zeta \tag{6.1}$$

Where ζ represents cluster density per square meter of rice crop within the sampling field. The Hydra probe time-domain reflectometry sensor is used for m_v measurements at $0-5\ cm$ depth. The $1m$ long metallic plate having $1cm$ horizontal and vertical grid lines is used to draw the surface roughness profile. Further, the surface roughness profile is digitized for the computation of s and l. The Gaussian autocorrelation function is used for the calculation of l.

6.3 Methodology

6.3.1 First order modified radiative transfer model

The presented study uses the first-order vector radiative transfer model to simulate the polarimetric bistatic scattering coefficients of the vegetation rough soil surface. The first-order vector radiative transfer model includes the following approximation, scattering parametrizations, and iterative techniques for solving vector radiative transfer equation (RTE). The vegetation canopy overlaying a rough surface is approximated as discrete spherical Rayleigh scatterers over a lossy surface such that the electromagnetic signal scattered by these particles has a random phase, thus allowing the addition of multiple contributions incoherently[173]. The random distribution of scattering constituents is assumed to have weakly scattering albedo ($w = \frac{k_s}{k_e} \leq 0.2$). k_s and k_e represent wave scattering and extinction coefficients in the vegetation medium. Roughness parameters

and moisture content characterize the lossy surface beneath vegetation foliage. The soil roughness is assumed to be temporally invariant to reduce model complexity.

The iterative technique for solving RTE starts with computing a zero-order solution, which further acts as a source function for the computation of a first-order solution. The computation of zero-order solution ignores vegetation constituents scattering, except for its loss due to absorption within the medium[3, 85, 94]. Thus, the expression of first-order total bistatic scattering coefficients solution (σ^0_{pq}) for BiSCAT configuration (i.e., downward incidence along ($\pi - \theta_i, \phi_i = 0$) and upward bistatic specular scattering along ($\theta_r = \theta_i, \phi_r = \phi_i = 0$)

$$\sigma^0_{pq} = \sigma^{AS}_{pq} + \sigma^V_{pq} \tag{6.2}$$

$$\sigma^{AS}_{pq} = \gamma^2 \sigma^S_{pq} \tag{6.3}$$

$$\sigma^V_{pq} = 4\pi \cos\theta_i [T_v]_{pq} \tag{6.4}$$

$$\gamma^2 = e^{\frac{-2\tau}{\cos\theta_i}} \tag{6.5}$$

Where γ^2 is the two-way wave attenuation in the vegetative medium. σ^{AS}_{pq} and σ^V_{pq} are the bistatic scattering coefficients of the rough soil surface scattering contriburion (i.e., σ^S_{pq}) attenuated by vegetarion foliage and vegetation foliage scattering contributions, respectively. τ is vegetation optical depth. The $[T_v]_{pq}$ is defined as the total first-order bistatic scattering contribution from the vegetated medium. The empirical relation between τ and PWC, as shown in Equation 6.6, is used to connect the model with vegetation biophysical parameters.

$$\tau = k_e d = C_{pq} PWC \tag{6.6}$$

The parameter C_{pq} is the empirical polarized frequency-specific parameter.

6.3.2 Kirchhoffs model for rough soil surface bistatic scattering

The choice of a bistatic scattering model for rough soil surface with as much realism is important to ensure the credibility and accuracy of the results. There are various rough soil surfaces bistatic scattering problems such as the small perturbation model, physical optics model, two-scale model, and Kirchhoff's model formulated under different validity conditions using the frequency, incidence/scattering angles, and soil roughness parameters (i.e., s and l)[54, 85, 174–176]. There is currently no general theory applied to the very rough surfaces since, as the surface roughness increases, the incoherent power reflected from the surface tends to increase. However, for slowly varying surfaces such as agricultural fields, the radius of curvature (R_c) is much greater than the wavelengths(λ); for such cases, the KA can be used to obtain a significant simple solution. The $kl > 6$ and $R_c > \lambda$ is the validity condition of KA as discussed in [85]. The KA employed the effect of roughness parameters on flat surface reflection coefficients. Therefore, the KA results do not include the complete polarization effect. The general expression of bistatic scattering coefficients for rough soil surface using KA is given as

$$\sigma_{pq}^{S} = \frac{k^2 \cos\theta_i^2}{\pi} R_{pq}^2 f^2 I \tag{6.7}$$

Where f and I are the fields in the KA and ensemble average of scattered intensity under the assumption that the soil surface is isotropic and homogeneous. K and R_{pq} represents the wavevector and Fresnels reflection coefficient.

The expression of f and I in KA are formulated as

$$f(\theta_i, \theta_r, \phi_r) = \frac{1 + \cos\theta_i \cos\theta_r - \sin\theta_i \sin\theta_r \cos\phi_r}{\cos\theta_i(\cos\theta_i + \cos\theta_r)} \tag{6.8}$$

$$I = \frac{\pi l^2}{v_z^2 s^2} e^{\left(-\frac{v^2 l^2}{4 v_z^2 s^2}\right)} \tag{6.9}$$

Where the expression of v_z, v, x and y is detailed in Chapter 21 by [85] and are defined as

$$v_z = -k(\cos\theta_i + \cos\theta_r) \tag{6.10}$$

$$v = x^2 + y^2 \tag{6.11}$$

$$x = k(\sin\theta_r \cos\phi_r - \sin\theta_i) \tag{6.12}$$

$$y = k\sin\theta_r \sin\phi_r \tag{6.13}$$

Thus, the bistatic scattering coeffficient of the rough soil surface in forward specular plane (i.e., θ_i=θ_r; ϕ_i = ϕ_r=0) is simplified as

$$\sigma_{pq}^S = \frac{l^2 R_{pq}^2}{4s^2} = \frac{R_{pq}^2}{2m^2} \tag{6.14}$$

Where m is the surface mean square slope which is defined as $\sqrt{2}\frac{s}{l}$. The above expression of bistatic scattering coefficients is not capable of yielding cross-polarized reflectivity polarization factors within the specular plane of incidence. The co-polarized Fresnels reflectivity is defined as

$$R_{HH}(\theta_i) = \frac{\cos\theta_i - \sqrt{\varepsilon' - \sin^2\theta_i}}{\cos\theta_i + \sqrt{\varepsilon' - \sin^2\theta_i}} \tag{6.15}$$

$$R_{VV}(\theta_i) = \frac{\varepsilon'\cos\theta_i - \sqrt{\varepsilon' - \sin^2\theta_i}}{\varepsilon'\cos\theta_i + \sqrt{\varepsilon' - \sin^2\theta_i}} \tag{6.16}$$

The value of soil dielectric constant (ε) in the Fresnels reflection coefficients is computed using the Dobson model.

6.3.3 Dobson model for relative soil dielectric constant

The semi-empirical model between the values of relative ε_m and m_v is initially proposed by [47]. The model uses the free space microwave transmission and waveguide approach to measure data of five different soil samples from 1.4 – 18 GHz. The model provides real and imaginary parts of soil dielectric, which are the functions of soil's textural composition (sand, silt, and clay fraction), bulk density (ρ_b), particle density (ρ_s), and the m_v content. The Dobson model was further improved by [155] for the low-frequency range, ranging from 0.3-1.3 GHz. The relative ε_m of soil moisture mixture has parameters that do not depend upon the specific soil type and can be theoretically expressed in terms of real ($\varepsilon_m^{'}$) and imaginary ($\varepsilon_m^{''}$) parts:

$$\varepsilon_m = \varepsilon_m^{'} + \varepsilon_m^{''} \tag{6.17}$$

$$\varepsilon_m^{'} = [1 + \frac{\rho_b}{\rho_s}\varepsilon_s^{\alpha} + m_v^{\beta'}\varepsilon_{fw}^{'\alpha} - m_v]^{\frac{1}{\alpha}} \tag{6.18}$$

$$\varepsilon_m^{''} = [m_v^{\beta''}\varepsilon_{fw}^{''\alpha}]^{\frac{1}{\alpha}} \tag{6.19}$$

Where α and β are the empirical modeled shape and texture factors, respectively. ε_s and ε_{fw} are the solid soil matter and free water dielectric constants.The measurement procedures of soil representatives such as sand, silt, clay, particle, and bulk density are detailed in [156]. The land surface parameters used in the computation of the real part of the dielectric constant are tabulated in Table 6.1.

Table 6.1 Land surface parameters

Depth (m)	Sand (%)	Silt (%)	Clay (%)	Bulk density (Mgm^{-3})	Particle density (Mgm^{-3})
0-0.20	12.8	65.1	22.1	1.49	2.58

6.3.4 Vegetation scattering components

The expression of $[T_v]_{pq}$ is obtained by solving vector RTE for downward incidence direction $(\pi - \theta_i, \phi_i)$ and upward bistatic specular scattering direction $(\theta_s = \theta_i, \phi_s = \phi_i)$ as discussed in [3]. Thus, the four first-order terms can be expressed as

$$[T_v]_{pq} = T_1^V + T_2^{S-V} + T_3^{V-S} + T_4^{S-V-S} \tag{6.20}$$

$$T_1^V = (1-\gamma^2)\frac{w}{2}P \tag{6.21}$$

$$T_2^{S-V} = \frac{d\gamma^2}{\cos\theta_i}\frac{R_{pq}}{2m^2}k_s P \tag{6.22}$$

$$T_3^{V-S} = \frac{d\gamma^2}{\cos\theta_i}k_s P\frac{R_{pq}}{2m^2} \tag{6.23}$$

$$T_4^{S-V-S} = \gamma^2(1-\gamma^2)\frac{w}{2}P(\frac{R_{pq}}{2m^2})^2 \tag{6.24}$$

On substituting Eqautions 6.21-6.24 in Equation 6.4, the mathematical expression of fisrt-order bistatic scattering contributios becomes

$$\sigma_{pq}^V = \sigma_1^V + \sigma_2^{S-V} + \sigma_3^{V-S} + \sigma_4^{S-V-S} \tag{6.25}$$

Where the various zero-order and first-order contributions are represented symbolically in the Figure 6.2. The first term (i.e., σ_1^V) in Equation 6.25 represents the single bistatic scattering contribution in the specular direction due to the vegetation medium, which does not contain the soil surface contribution. The second and third terms (i.e., σ_2^{S-V} and σ_3^{V-S}) represent single bistatic scattering due to the vegetation medium, which is further reflected in the forward specular direction by the soil reflection and vice versa. The last term (i.e., σ_4^{S-V-S}) represents the single vegetation scattering and double soil surface reflection in the forward specular direction. The bottom layer is assumed to be a rough surface and temporally invariant. Therefore, the soil roughness parameter affecting the soil reflectivity

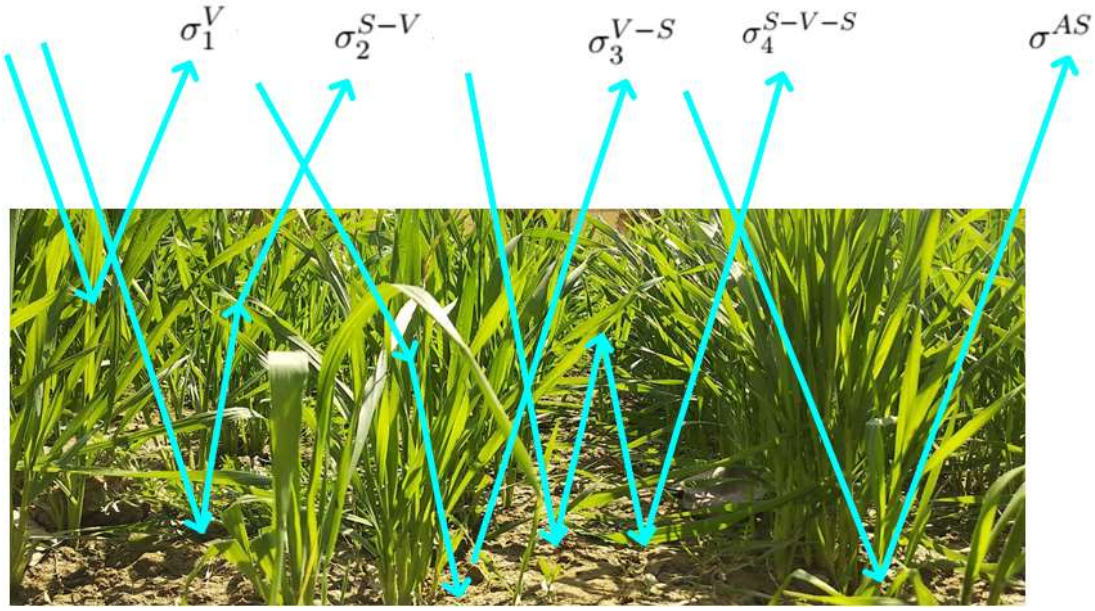

Fig. 6.2 Visualization of the zero and First-order bistatic scattering contributions

in a specular direction is taken into account as derived from the Kirchhoffs model. The scattering pattern of the vegetation constituents in the scattering model is described by the Rayleigh phase function (i.e., P) as shown in Equation 6.26.

$$P = \frac{3}{16\pi}(1+\cos\Phi^2) \tag{6.26}$$

$$\cos\Phi = \cos\theta_i\cos\theta_r + \sin\theta_i\sin\theta_r\cos(\phi_i - \phi_r) \tag{6.27}$$

The scattering generalization parameter (i.e., $\cos\Phi$) in Equation 6.27 is represented in terms of scalar product between transmitting and scattered wave vector. The expression of vegetation constituents scattering coefficient (i.e., k_s) are simplified using Equation 6.28,

$$k_s = wk_e = \frac{w\tau}{d} = \frac{wC_{pq}PWC}{d} \tag{6.28}$$

6.4 Results and discussion

6.4.1 Experimental assessment and optimization of the BiSCAT system

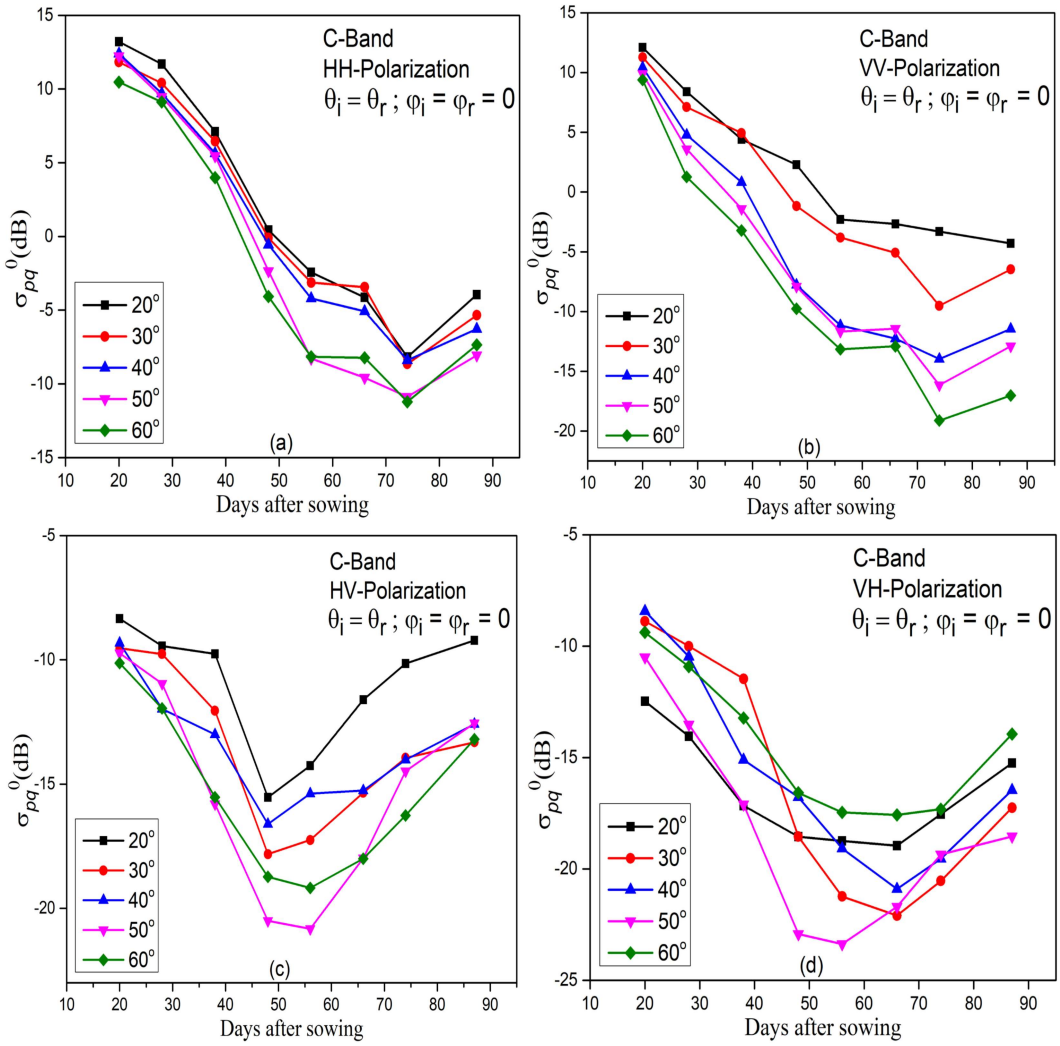

Fig. 6.3 (a)-(d) The temporal and multi-angular behavior of measured bistatic scattering coeffiecient curves at C band for HH, VV, HV and VH polarizations.

The fully polarimetric bistatic scattering from vegetation (i.e., wheat crop) overlaying rough soil surface in the specular plane was measured using the BiSCAT system at C band. The temporal (i.e., 20 DAS to 67 DAS) and multi-angular (i.e., 20° to 60°) behavior of

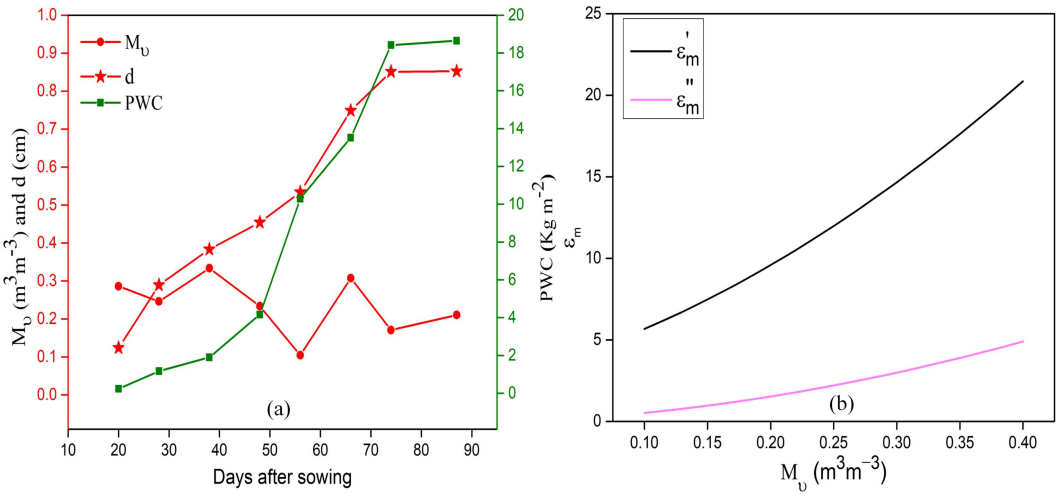

Fig. 6.4 (a) The temporal variation of the insitu land bio-geophysical parameters; (b) Variation of soil dielectric constant(ε_m) with m_v

measured bistatic scattering coefficient curves at the C band for HH, VV, HV, and VH polarizations are plotted in Figures 6.3 (a)-(d). The experimental assessment of polarimetric BiSCAT measurements is based on the temporal variation of the σ^0_{pq} curves with the land bio-geophysical parameters. The temporal variation of the land bio-geophysical parameters, namely, PWC, d, and m_v and computation of soil dielectric constant using the Dobson model are shown in Figures 6.4 (a) and (b).

The approximate decreasing trend of the co-polarized $\sigma^0_{HH/VV}$ is reported with the increase in PWC and d till the grain filling stage (i.e., 74 DAS) of the wheat crop. This is due to the temporal extinction (i.e., scattering and absorption loss) in the co-polarized electromagnetic signal provided by the temporal change in the vegetative growth parameters. However, after the grain filling stage, the measured values of co-polarized $\sigma^0_{HH/VV}$ are found to increase slightly. The defoliation of emerging leaves, maturity of vegetation growth parameter, and inclination of the plant might be the significant reason behind the increase in the amplitude of co-polarized $\sigma^0_{HH/VV}$ after the grain filling stage of wheat crop. The influence of m_v is not found efficiently on the temporal curves of σ^0_{pq} for the vegetated terrain. Therefore, the conclusion can be made that the penetrating power of the C band

is viable for vegetation information retrieval. In contrast, the cross-polarized temporal curves of measured σ^0_{HV} are found to decrease approximately till the booting stage of the wheat crop (i.e., between 48 to 51 DAS). However, the approximate decreasing trend of cross-polarized σ^0_{VH} is reported till the heading stage of the wheat crop (i.e., between 57 to 65 DAS). The decrease in σ^0_{VH} till the heading stage compared to σ^0_{HV} is due to the higher loss of vertically polarized microwave electromagnetic incidence signals with the vertically oriented stalks of the wheat crop. However, after the decreasing trend, the temporal curves of measured $\sigma^0_{HV/VH}$ increased. The anamoly of temporal variation of $\sigma^0_{HV/VH}$ might be understood by taking the vegetation optical depth(VOD) and scattering albedo into account. Since at the early booting stages, the wheat crops have had minimal scattering due to the lower VOD and w. Therefore, depolarization/change in polarization of the incidence microwave electromagnetic signals is negligible, leading to the decrease of $\sigma^0_{HV/VH}$ curves. However, approximately after the late booting stage or the heading stage of the wheat crop (i.e., from 50 to 66 DAS), the higher VOD and w cause increased depolarization/change in polarization of electromagnetic signals, resulting in the increase in the temporal curves of $\sigma^0_{HV/VH}$.

The optimization of the BiSCAT measurement system was performed based on the correlation analysis. The correlation analysis facilitates finding the most suitable/sensitive specular incidence angle and polarization for monitoring land bio-geophysical parameters. The correlation value between the temporal curves of fully-polarized σ^0_{pq} and land bio-geophysical parameters (i.e., PWC and m_v) is tabulated in Table 6.2. The fully-polarimetric curves of σ^0_{pq} were found to be highly correlated with PWC and m_v at 30° specular angle of incidence. In particular, a high correlation between σ^0_{pq} with PWC and m_v was reported for HH-polarization with $R = 0.9244$; and $R = 0.5458$, respectively. Therefore, the C band at 30° specular incidence angle can be chosen as optimized parameters of the BiSCAT measurement system. The optimized specular incidence angle is further used to simulate

the value of co-polarized σ^0_{pq}. Since the KA uses the flat surface reflection coefficient to model the co-polarized effect from the soil surface, it does not include the cross-polarized effect. The presented study in this article is limited to simulating the co-polarized value of $\sigma^0_{HH/VV}$.

Table 6.2 Correlation analysis between 8-measured fully-polarimetric σ^0_{pq} with PWC and m_v

Incidence angle			20°	30°	40°	50°	60°
C-band	HH	PWC	-0.9110	**-0.9244**	-0.9183	-0.8971	-0.8774
		m_v	0.5066	**0.5458**	0.5242	0.5411	0.5412
	VV	PWC	-0.9052	**-0.9185**	-0.8740	-0.8797	-0.8945
		m_v	0.4852	**0.5319**	0.5060	0.5304	0.5283
	HV	PWC	-0.0304	**-0.4135**	-0.3497	-0.1734	-0.3322
		m_v	0.4176	**0.4727**	0.3390	0.3169	0.3465
	VH	PWC	-0.4018	**-0.7621**	-0.7417	-0.5157	-0.6448
		m_v	0.2550	**0.5147**	0.3545	0.4461	0.4530

6.4.2 Model calibration/validation datasets generation and optimization

A total of the 8-BiSCAT observations and in-situ parameters (i.e., PWC, d, and m_v) were linearly regressed at 1-day intervals over different phenological stages of the wheat crop. A total of 68 datasets, including measured σ^0_{pq} at 30° specular incidence angle, PWC, d, and m_v on a daily basis, were generated for model parameters optimization. 75 % of the total datasets are used for model calibration. In comparison, the remaining 25 % is used to validate the accuracy of the model. The constrained non-linear least square optimization technique is used to calibrate/optimize the model parameters, namely C_{pq} and w. This technique minimizes the defined cost function as shown in Equation 6.29 to find the optimum model parameters.

$$cost = min|\sum_{i=0}^{n}(measured\ \sigma^0_{pq_i} - simulated\ \sigma^0_{pq_i}(C_{pq}, w))^2| \tag{6.29}$$

The optimal condition of the first-order microwave RTM parameters, namely C_{pq} and w are constrained to be bound between $0 < C_{pq} < 1$ and $0 < w < 0.2$, respectively. The obtained values of optimized model parameters are shown in Table 6.3.

Table 6.3 Optimized model paramters

Band	Polarization	C_{pq}	w
C-band	HH	0.1189	0.0795
	VV	0.1333	0.1489

6.4.3 Simulation results

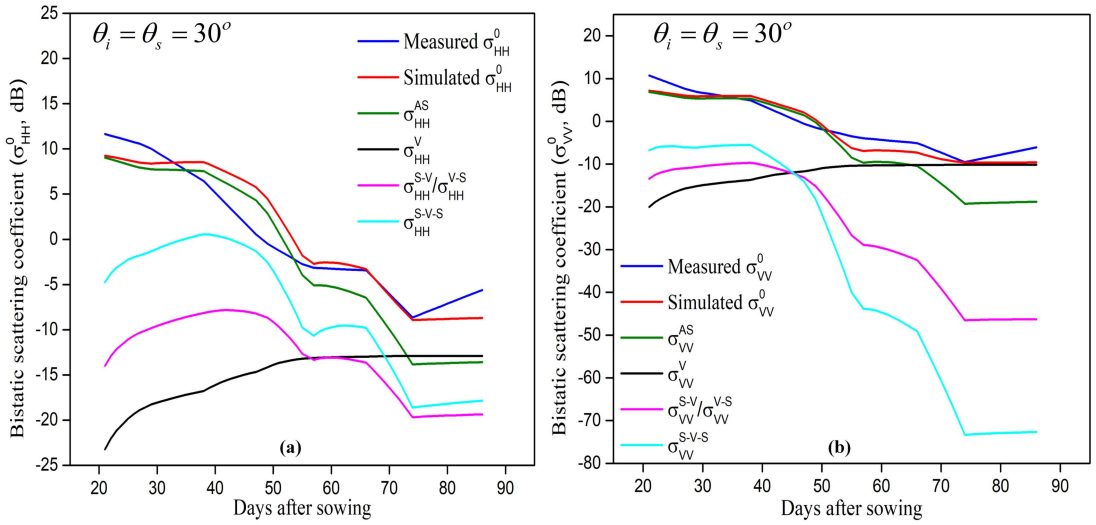

Fig. 6.5 The simuluted results of co-polarized $\sigma^0_{HH/VV}$ using PWC as an auxiliary dataset for C band .

In general, the total value of $\sigma^0_{HH/VV}$ can be formulated using the coherent scattering component and incoherent scattering components. However, due to the lower penetrating power of the C band, the coherent scattering component is assumed to be negligible compared to the incoherent scattering components. Therefore, the insights of the total $\sigma^0_{HH/VV}$ in the presented study are analyzed based on the dominance of the incoherent scattering components within total values of simulated $\sigma^0_{HH/VV}$. The simulation of co-polarized $\sigma^0_{HH/VV}$ at 30° specular incidence angle for the C band was performed using PWC

as auxiliary datasets in the first-order modified radiative transfer model. The contribution of incoherent scattering components, for instance, attenuated direct soil scattering component ($\sigma^{AS}_{HH/VV}$), direct vegetation scattering component($\sigma^{V}_{HH/VV}$), soil-vegetation/vegetation-soil interaction scattering component($\sigma^{S-V/V-S}_{HH/VV}$) and soil-vegetation-soil interaction scattering components($\sigma^{S-V-S}_{HH/VV}$) within the total value of simulated $\sigma^{0}_{HH/VV}$ is plotted in Figures 6.5 (a) and (b). Since the vegetation is assumed to have weakly scattering albedo, the σ^{AS}_{pq} scattering component was found to be the dominant contribution within the simulated σ^{0}_{pq} for both HH and VV polarization. The obtained values of simulated σ^{0}_{HH} were found to be higher compared to the simulated σ^{0}_{VV}. This is due to contribution of first-order and first-order interaction components (i.e., σ^{V}_{pq}, $\sigma^{S-V/V-S}_{pq}$, and σ^{S-V-S}_{pq}) for HH-polarization is found to have higher values compared to VV-polarization. The above result confirms that the extinction of vertically polarized electromagnetic signals due to the interaction with the wheat crop's vertically oriented lossy dielectric stalks is higher than Horizontally polarized electromagnetic signals. As the vegetation biophysical parameter increases, the contribution of $\sigma^{V}_{HH/VV}$ within the simulated $\sigma^{0}_{HH/VV}$ also increases. The contribution of σ^{V}_{HH} scattering component is found dominant after the 56, 70 and 74 DAS compared to $\sigma^{S-V/V-S}_{HH}$, σ^{S-V-S}_{HH} and σ^{AS}_{HH}, respectively, as shown in Figure 6.5(a). In contrast, the early dominance of σ^{V}_{VV} is reported due to the higher loss of vertically polarized electromagnetic signal in the vegetative medium, as shown in Figure 6.5(b). The contribution of σ^{S-V-S}_{HH} and $\sigma^{S-V/V-S}_{HH}$ is found to be the second and third most significant contributions to the 56 and 70 DAS within the simulated σ^{0}_{HH}, respectively. Similarly, the contribution of σ^{S-V-S}_{VV} and $\sigma^{S-V/V-S}_{VV}$ is found to be the second and third most significant contributions to the 46 DAS within the simulated σ^{0}_{VV}, respectively. After the 46 DAS, the contribution of $\sigma^{S-V/V-S}_{VV}$ is found to be higher compared to the σ^{S-V-S}_{VV} component contribution.

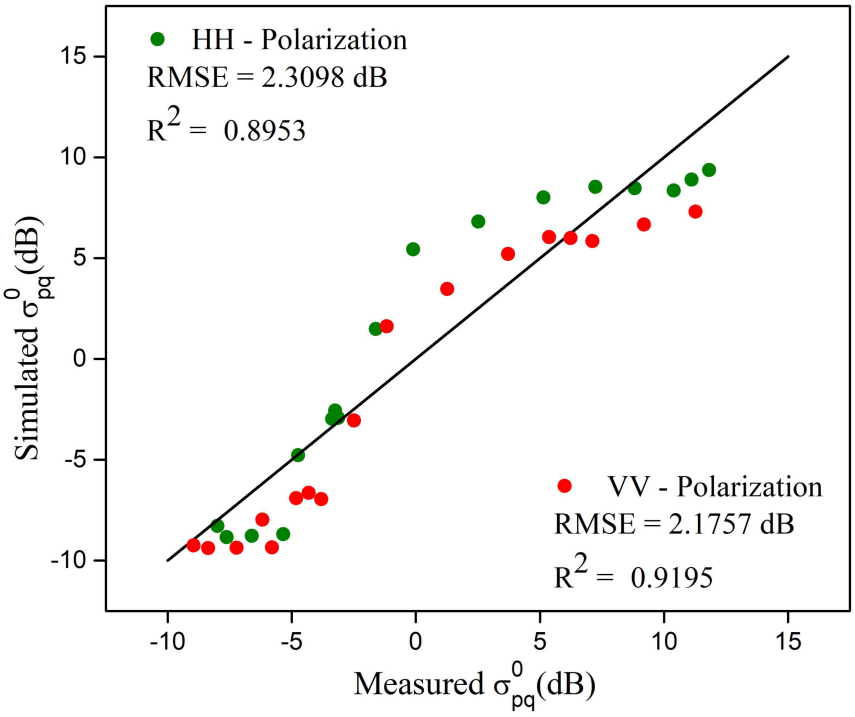

Fig. 6.6 The Q:Q plot between simulated $\sigma^0_{HH/VV}$ using the optimized modified radiative transfer model and measured σ^0_{pq}.

6.4.4 Model validation

The performance of optimized model parameters in the calibrated first-order MRTM is used to validate the simulated σ^0_{pq} with the measured observation. The Q:Q plot between simulated and measured σ^0_{pq} is shown in Figure 6.6. The indices, namely, root mean square error (RMSE) and squared correlation coefficients (R^2) are used to evaluate the performance of optimized first-order RTM. The temporal curve of simulated σ^0_{VV} from the first-order MRTM using PWC as an auxiliary dataset performs better with Low RMSE = 2.1757 dB and high R^2=0.9195 compared to the value of simulated σ^0_{HH}. The performance indices of simulating σ^0_{pq} from the presented microwave scattering algorithm using PWC as an auxiliary dataset yeild good agreement with the measured σ^0_{pq} and are practically viable for bistatic geometric configuration.

6.5 Conclusion

In the presented study, the potential of the fully polarimetric bistatic radar returns measured from the designed BiSCAT system over a wide specular incidence angular range for monitoring wheat crop growth at the C band was evaluated. The experimental assessments of variation in the temporal and multi-angular bistatic radar returns were performed based on the temporal variation of vegetation and land surface properties. The temporal scattering responses at various specular incidence angles ranging from 20° to 60° at an interval of 10° were optimized based on correlation analysis between σ^0_{pq} with PWC and m_v. The correlation analysis showed that a 30° specular incidence angle was found optimum for the BiSCAT system.

The interpretation of bistatic scattering returns was evaluated utilizing the synergy of the rough soil surface scattering model in the first-order radiative transfer model-based vegetation scattering model. The KA was used to mimic co-polarized scattering response of rough soil surface in a specular direction. However, the KA model is limited to providing insights into co-polarized radar return from the target due to the incapability of yielding the cross-polarization factor in the forward specular plane of incidence. In addition, the Rayleighs phase function approximates the scattering pattern of vegetation constituents within the presented model. The interpretation of simulated values of σ^0_{pq} is entirely based on the decomposition of scattering contribution and their dominance at different stages of the vegetation growth period. The temporal dynamics simulated σ^0_{pq} were modeled by introducing the empirical relation between VOD and PWC. The performance indices between measured and simulated σ^0_{pq} showed that the developed first-order RTM acts as an excellent simulator for modeling bistatic radar response in a physical scattering way. The future studies of the presented work are as follows: (1) Modeling and evaluation of cross-polarized bistatic scattering sensitivity to vegetation, and (2) Designing the BiSCAT measurement system having both the zenith and azimuth

variation to obtain the multidirectional information of vegetation and optimum parametric configuration for vegetation monitoring.

****